2023-01-1643 Published 31 Oct 2023



Investigation of Performance of Fischer-Tropsch Coal-to-Liquid Fuel, IPK, in a Common Rail Direct Injection Compression Ignition Research Engine with Varying Injection Timing

Valentin Soloiu, James Willis, Amanda Weaver, Brandon O'Brien, Nicholas Dillon, and Zachary Davis Georgia Southern University

Citation: Soloiu, V., Willis, J., Weaver, A., O'Brien, B. et al., "Investigation of Performance of Fischer-Tropsch Coal-to-Liquid Fuel, IPK, in a Common Rail Direct Injection Compression Ignition Research Engine with Varying Injection Timing," SAE Technical Paper 2023-01-1643, 2023, doi:10.4271/2023-01-1643.

Received: 15 Jun 2023 Revised: 08 Aug 2023 Accepted: 21 Aug 2023

Abstract

n investigation of the performance and emissions of a Fischer-Tropsch Coal-to-Liquid (CTL) Iso-Paraffinic Kerosene (IPK) was conducted using a CRDI compression ignition research engine with ULSD as a reference. Due to the low Derived Cetane Number (DCN), of IPK, an extended Ignition Delay (ID), and Combustion Delay (CD) were found for it, through experimentation in a Constant Volume Combustion Chamber (CVCC). Neat IPK was analyzed in a research engine at 4 bar Indicated Mean Effective Pressure (IMEP) at three injection timings: 15°, 20°, and 25° BTDC. Combustion phasing (CA50) was matched with ULSD at 10.8° and 16° BTDC. The IPK DCN was found to be 26, while the ULSD DCN was significantly higher at 47 in a PAC CID 510. In the engine, IPK's DCN

combined with its short physical ignition delay and long chemical ignition delay compared to ULSD, caused extended duration in Low Temperature Heat Release (LTHR) and cool flame formation. It was found in an analysis of the Apparent Heat Release Rate (AHRR) curve for IPK that there were multiple Negative Temperature Coefficient (NTCR) regions before the main combustion event. The High Temperature Heat Release (HTHR) of IPK achieved a greater peak heat release rate compared to ULSD. Pressure rise rate for IPK was observed to increase significantly with increase in injection timing. The peak in-cylinder pressure was also greater for IPK when matching CA50 by varying injection timing. Emissions analysis revealed that IPK produced less NO_x , soot, and CO_2 compared to ULSD. CO and UHC emissions for IPK increased.

Introduction

s concerns over climate change and energy security continue to rise, the research and development of sustainable synthetic alternative fuels has emerged as a viable solution. These sustainable and clean-burning fuels have potential as a supplement or "drop-in" replacement of typical petroleum fuels with minimal reconfiguration of combustion engines or infrastructure. Alternative fuels can be produced from a variety of resources and can be blended into typical fuels for on-road or aviation applications [1, 2, 3, 4].

Created using the Fischer-Tropsch process, these alternative fuels are cleaner fuels with promising emissions profiles compared to existing fuels [5, 6, 7]. They are created using feedstocks such as coal, natural gas, and biomass, promoting energy independence. These feedstocks are common due to the adequate number of hydrocarbons in their composition. The properties of synthetic fuels are contingent on the type and condition of the feedstock used in its creation [8, 2]. The synthetic fuel investigated in this paper is Iso-Paraffinic

Kerosene (IPK), produced from a coal feedstock. IPK has already seen commercial use since 1999, when Sasol, the producer of IPK, was given permission to blend IPK into conventional petroleum-based jet fuels in South Africa [10]. Additionally, the production of a generic synthetic paraffinic kerosene (SPK) produced by the United States Air Force in 2009 and continued research into synthetic alternatives showcases the demand and efficacy of synthetic fuel applications [11, 12, 13].

IPK is primarily made of branched chain hydrocarbons known as iso-paraffins and due to the purity of fuels produced by the Fischer-Tropsch process, lacks aromatics and significant sulfur content. Low levels of aromatics are related to decreased heats of vaporization and viscosity, while low sulfur content is related to decreased lubricity [14, 15]. Another noteworthy attribute of IPK is the length of its combustion and of its negative temperature coefficient region (NTCR).

An investigation of IPK was conducted by Xin Hui et al. [11] in a fuel ignition tester based on ignition and combustion

delay, autoignition characteristics and laminar flame profile. It was found that IPK had a much longer ignition and combustion delay and decreased DCN than any other fuel tested. Additionally, IPK displayed the slowest flame stretch and extinction rates across all tested equivalence ratios, which is attributed to iso-paraffins being its primary composition [16, 17, 18, 19, 20, 21].

Previous investigations on IPK were performed by Soloiu et al in a constant volume combustion chamber and in a single-cylinder indirect injection (IDI) engine. The goal of these studies was to develop a detailed understanding about the thermophysical properties and combustion characteristics of IPK as a fuel. ULSD was used in both cases as a baseline to compare to. It was found that IPK showed a significant decrease in NO_x, unburned hydrocarbons (UHC), and CO₂ emissions. Additionally, IPK was found to have a higher energy density and thermal efficiency [22, 23, 24, 25].

Combustion phasing, also known as ignition timing, is a measure of when combustion begins in an engine. The timing of ignition is a vital parameter to analyze and is directly related to the thermal efficiency and performance of the engine [26, 27, 28]. Comparing fuels based on injection timing provides some insight into the fuel properties. However, this form of analysis alone ignores fuel properties such as ignition delay, autoignition quality, and flame propagation. By varying the injection timing to match the combustion phasing, a more precise comparison can be made that accounts for these properties [29, 30, 31, 32].

In this investigation, F-T CTL fuel, the IPK, was analyzed using laboratory equipment to determine thermophysical and chemical properties such as vaporization behavior, atomization characteristics, DCN, ignition delay, and combustion delay in CVCC with ULSD as a baseline. Furthermore, IPK was run in a single cylinder CRDI engine at a constant load and 3 injection timings and compared with ULSD at matching injection timing and matching combustion phasing. Emissions and efficiency of the engine were studied to determine the efficacy of IPK as an alternative fuel for use in IC engines.

Thermophysical Properties

A number of experimental investigations were carried out using the authors' fuel analysis equipment to compare the thermophysical properties of IPK to ULSD. These investigations provide critical insight into the physical and chemical properties of the fuels which have direct implications for combustion in the CVCC as well as in the engine. A thermogravimetric analysis and differential thermal analysis were performed to analyze the rate of vaporization and low temperature oxidation behavior of the fuels, both of which have an effect on the physical ignition delay of the fuels. Further investigations were carried out to determine the spray droplet size and distribution, which also has significant implications for the physical ignition delay of the fuel [33, 34, 35].

Using a Constant Volume Combustion Chamber (CVCC), the Ignition Delay (ID) and Combustion Delay (CD), as well as the Derived Cetane Number (DCN) were evaluated. The Lower Heating Value (LHV) was determined using a Parr

1341 constant volume digital calorimeter. Viscosity of the fuels was measured using a Brookfield DV-II +Pro rotational viscometer. Viscosity also plays an important role in the droplet formation and mixing capabilities of the fuels. A summary of these parameters is provided below in <u>Table 1</u>.

Additionally, the chemical composition for IPK compared to ULSD is provided below in <u>Table 2</u>, which provides valuable context to the chemical analysis further in the paper.

Thermal Stability and Low Temperature Oxidation

An analysis was conducted to determine the oxidation at low temperatures and volatility of IPK and ULSD. This investigation was done by placing approximately 10 mg of research fuel in the Shimadzu DTG-60. This instrument is used to perform thermogravimetric analysis (TGA) and differential thermal analysis (DTA). The furnace was heated from 20°C to 600°C in 20°C increments per minute. A constant air flow rate of 15 mL/min was supplied to the furnace chamber in order to promote fuel oxidation and purge the created oxidation fumes. This sample is weighed against and compared to a baseline sample of alumina powder of similar mass. This material is chosen due to its refractory nature and negligible loss in mass as the chamber is heated and cooled.

Thermogravimetric analysis in the DTG is used to measure the vaporization rate of the research fuel by measuring percent mass reduction with respect to temperature. As shown in <u>Fig. 1</u>, IPK is shown to vaporize much faster than ULSD, indicating a much higher volatility. Fuels with high volatility form a more homogeneous fuel-air mixture in less time and at lower temperatures than low volatility fuels [39, 40].

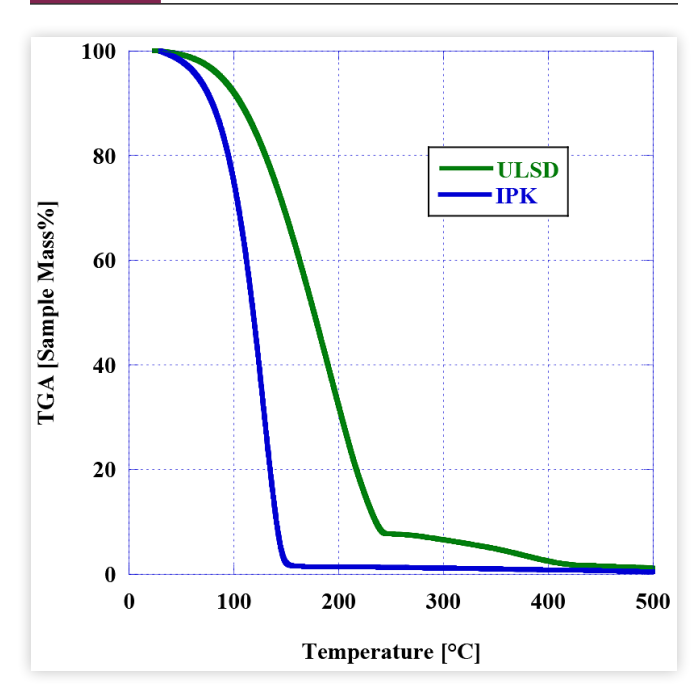
TABLE 1 Thermophysical Properties of IPK compared to ULSD [36]

	IPK POSF7629 / ± %diff Compared to ULSD	ULSD
LHV (MJ/kg)	44.25 / +7.66	41.1
DCN	25.88 / -46.71	48.56
Avg. ID (ms)	5.3 / +53.18	3.46
Avg. CD (ms)	17.2 / +247.47	4.95
Viscosity @ 40°C (cP)	1.02 / -58.20	2.44
Density @ 26°C (kg/m³)	740 / -12.94	850
SMD [μm]	14.96 / -33.09	22.36

TABLE 2 Chemical composition of IPK compared to [36, 37, 38]

Composition	Sasol IPK / ± %diff	ULSD
n-Paraffins (wt%)	2.1 / -87.20	16.4
Iso-paraffins (wt%)	88 / +378.26	18.4
Cyclo-paraffins (wt%)	9 / -74.29	35
Aromatics (wt%)	<0.5 / -98.33	30
Total sulfur (wt%)	<0.001 / -99.99	<15





The results of the thermogravimetric analysis can be more precisely found in <u>Table 3</u> below, where the temperature required to vaporize 10%, 50%, and 90% of the fuel is recorded. These temperatures are labeled as TA(10), TA(50), and TA(90) respectively. Near the beginning of the analysis, at approximately TA(10), ULSD and IPK require similar temperatures in order to vaporize, less than a 30° difference. However, as the analysis continued, IPK required significantly lower temperatures than ULSD in order to vaporize the same amount.

The differential thermal analysis in the DTG is used to quantify the absorption and release of energy in terms of temperature. This analysis is able to determine endothermic and exothermic processes that take place over a 600°C temperature range. In differential thermal analysis, endothermic reactions are represented by a negative slope and exothermic reactions are represented by a positive slope. The magnitude of the slope represents the rate at which these reactions take place. Fig. 2 below shows the DTA results of the two research fuels.

TABLE 3 Thermogravimetric Analysis of ULSD and IPK [36]

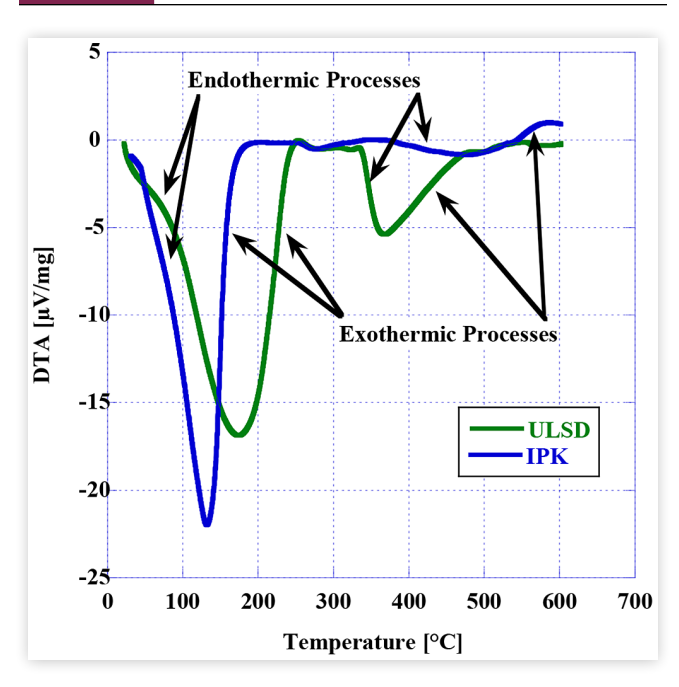
	IPK	ULSD
TA (10) °C	71.7	100.0
TA (50) °C	108.1	170.0
TA (90) °C	131.2	230.2

The DTA results show that at low temperatures, from 0°C - 250°C, both IPK and ULSD are very volatile. This is proven by the large endothermic reactions at the start of the analysis. These endothermic reactions, indicating a vaporization phase change, are likely due to the shorter and lighter hydrocarbon chains such as n- and iso-paraffins vaporizing at lower temperatures than other compounds [41]. It is observed that IPK is vaporizes sooner than ULSD given that IPK reaches a more negative peak than ULSD, sooner and at a steeper slope. Due to iso-paraffins being the primary compound of IPK, the extreme endothermic reaction in the beginning followed by little to no volatility across increasing temperatures was expected. Alternatively, ULSD has a significantly decreased amount of n- and iso-paraffins and exhibits a decreased volatility in the temperature range.

In mid temperature ranges (250°C - 350°C), IPK is shown to have low reactivity, with little to no reactions besides a small reaction at the upper end of the temperature range. ULSD, on the other hand, undergoes a significant endothermic reaction while IPK remains unreactive. This indicates low-temperature oxidation of hydrocarbon chains that are not present in IPK, such as aromatic compounds. Because of the lack of reactions in IPK at this temperature, IPK is shown to be the least reactive fuel in mid-range temperatures.

Lastly, in high temperature ranges (350°C+), IPK undergoes a small endothermic reaction that begins at approximately the same temperature ULSD reaches a peak in its reaction. After this temperature, ULSD follows a gentle slope instead of a steep one like the first reaction and eventually lines up with the end of the IPK endothermic reaction. This suggests that near the peak of the second significant endothermic reaction in ULSD, the oxidation of other compounds began to take place, slowing the return of the endothermic reaction and preventing it from returning to zero. Additionally, the compounds that begin oxidizing in this temperature range

FIGURE 2 Differential Thermal Analysis of ULSD and IPK



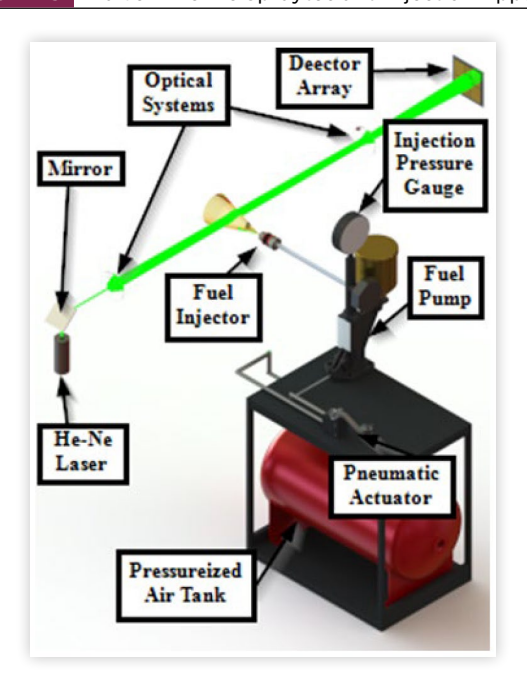
must be similar to those present in IPK due to the identical trend at the end of the fuels' reactions.

The differences in the DTA for IPK and ULSD can likely be attributed to ULSD having more prevalent and heavier hydrocarbons than IPK [36]. Overall, IPK was found to be much more volatile than ULSD, especially at lower temperature regions. However, ULSD was observed to be more reactive overall than IPK.

Spray Atomization, Mixing, and Droplet Distribution Analysis with Mie Scattering Laser Apparatus

The investigation into the droplet distribution, spray atomization, and mixture formation for neat IPK and neat ULSD was conducted using a Malvern Spraytec He-Ne laser. When an injection was initiated, a laser beam is used to provide real-time measurement of the spray particle and spray droplet size distribution. The instrument can be seen in Fig. 3 below. A 180 bar hydraulic injector was placed 100 mm from the laser beam.

FIGURE 3 Malvern He-Ne Spraytec and Injection Apparatus



There are twenty-eight light detectors reporting data at 10 kHz from 0.1 ms before trigger to 5 ms after trigger. The Mie Scattering and Fraunhofer diffraction theory were used to analyze the data by determining the Sauter Mean Diameter (SMD) and its spray droplets as a result of the diffraction of the laser.

The Mie Scattering Theory is a technique that describes the scattering of light off a particle cloud. Equation 1 allows for determination of the Sauter Mean Diameter (SMD) where $I(\theta)$ represents the light intensity after scattering as a function of the angle of incidence θ (the angle where the light hits the

droplet relative to where it was detected). The measured distance between the light detector and light source is represented by a, while the wave number in in $2\pi/\lambda$ is represented by k. $S_1(\theta)$ and $S_2(\theta)$ represent complex, dimensionless functions which account for the amplitude change of the perpendicular and parallel polarized light. I_0 describes the initial intensity of the beam $[\underline{42}]$.

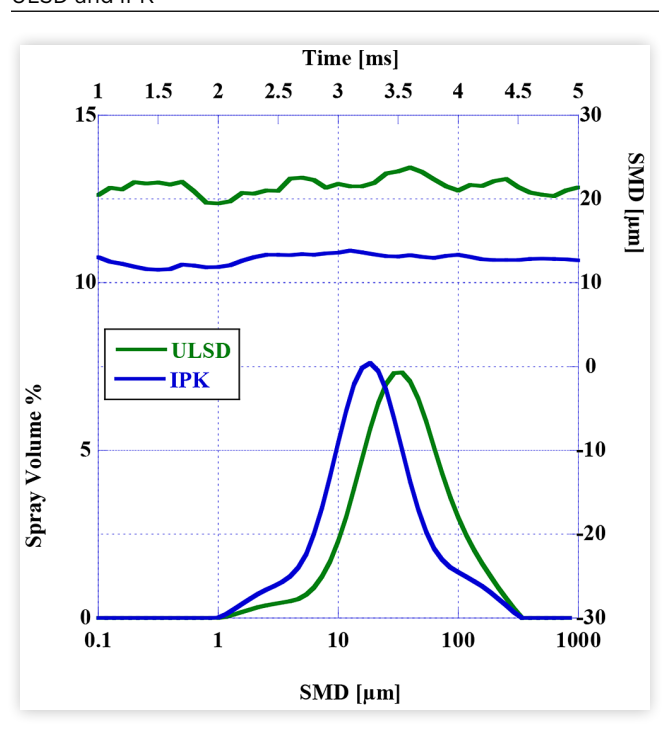
$$I(\theta) = \frac{I_0}{2k^2a^2} \left(\left[S_1(\theta) \right]^2 + \left[S_2(\theta) \right]^2 \right) \tag{1}$$

Equation 1 is well suited for spherical droplets, however in practice droplets are rarely perfectly spherical. Therefore, the Fraunhofer diffraction theory is applied since it does not rely on the optical properties of the droplet, or the sphericity of the droplet (Equation 2). The terminology is the same as Equation 1, with the addition of the dimensionless parameter $\alpha = \pi x/\lambda$, in which x is the particle size.

$$I(\theta) = \frac{I_0}{2k^2a^2}\alpha^4 \left(\frac{J_I(\alpha sin(\theta))}{\alpha sin sin \theta}\right)$$
 (2)

For the fuels selected, Sauter Mean Diameter (SMD) and Spray Droplet Distribution (SDD) were measured to generate the spray profile of each fuel. These results can be seen in Fig. 4. The lowest droplet size that was calculated from the neat tests was IPK. This is in part due to ULSD having a higher viscosity when compared to IPK, resulting in a droplet distribution skewed toward higher droplet diameter. IPK's physical properties are therefore seen to be favorable for spray atomization.

FIGURE 4 Spray Development and Droplet Formation for ULSD and IPK



Combustion Characteristics in a Constant Volume Combustion Chamber

The constant volume combustion chamber experiments were conducted using a Petroleum Analysis Company (PAC) CID 510. This instrument allowed for analyses for each fuel's pressure trace, heat release, ignition delay, combustion delay, low temperature heat release, and high temperature heat release. The PAC CID 510 typically operates by cycling through 5 condition periods where fuel is injected, it combusts, and exhausts. Following the conditioning periods are 15 combustion cycles in which measurements are taken. The pressure data for each of the 15 cycles is recorded and averaged. These test cycles are in line with ASTM standard D7667-14a, as shown in Table 4.

The schematic shown in <u>Fig. 5</u> depicts the components of the PAC CID 510. The right-hand image, the cross-sectional view, shows the common rail fuel injection system (labeled 1), with the 6 orifice Bosch high-pressure fuel injector (2).

The combustion takes place in the uniformly heated, constant volume, and pressure-controlled combustion chamber (3) shown in the left-hand image of Fig. 5. The pressure sensor, labeled 4, is the device that measures the difference of pressure during combustion. Finally, labeled 5, an additional pressure sensor is used to measure the in-line fuel pressure.

The DCN values given in <u>Table 5</u> were calculated with <u>Equation 4</u> below using the durations of ignition delay and combustion delay measured by the instrument. This equation comes from an in-house optimization by the authors, based on specific experimentation of the fuels presented in this

TABLE 4 CVCC Parameters based on ASTM D7668-14a

Wall	Fuel Injection	Coolant	Injection	Chamber
Temp.	Pressure	Temp.	Pulse Width	Pressure
595.5 °C	1000 bar	50 °C	2.5 ms	20 bar

FIGURE 5 PAC CID 510 Constant Volume Combustion Chamber Schematic

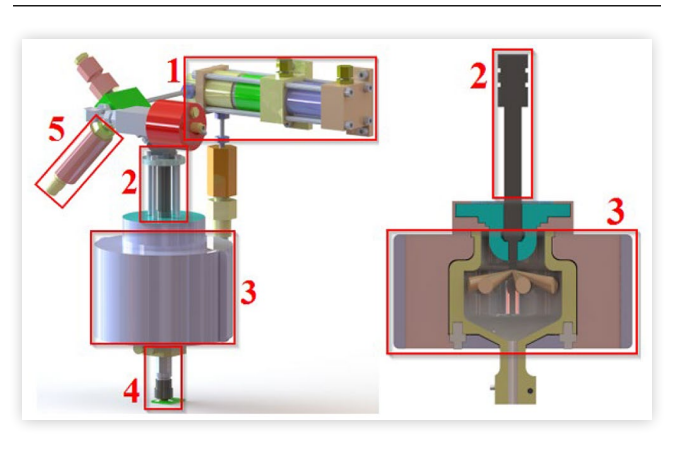


TABLE 5 ID, CD, and DCN for IPK compared to ULSD

Fuel	ID	CD	DCN
IPK / %diff	5.30 / +49%	17.17 / +233%	25.88 / -45%
ULSD	3.56	5.15	47

paper. It is loosely based off the generalized equation given by the instrument's manufacturer, Petroleum Analysis Company, that was derived for a large range of fuels. It is evident that due to IPK's extended ID and CD (49% and 233% greater, respectively) compared to ULSD are responsible for the low DCN of 25.88, 45% less than ULSD used in this investigation.

$$DCN = 13.028 + \left(-\frac{5.3378}{ID}\right) + \left(\frac{300.18}{CD}\right) + \left(-\frac{12567.90}{CD^2}\right) + \left(\frac{3415.32}{CD^3}\right)$$
(4)

Combustion Pressure and Ringing Analysis in the CVCC

The pressure trace for both research fuels were recorded in the PAC CID 510, averaged, and compiled together in <u>Fig. 6</u>. This parameter, excluding time, is the only parameter measured by the CVCC. Further analysis is derived from this measured pressure. Start of injection in the CVCC occurs at 0ms.

The pressure results show the extended combustion duration of IPK compared to ULSD. Further combustion duration analysis is explored below.

Using the pressure trace, the ringing intensity of each research fuel can be investigated as well. Shown in <u>Fig. 7</u> are the pressure trace curves of both fuels at their peaks, using a logarithmic scale for easier analysis. It can be seen in the figure

FIGURE 6 Combustion Chamber Pressure Traces of Neat IPK and Neat ULSD

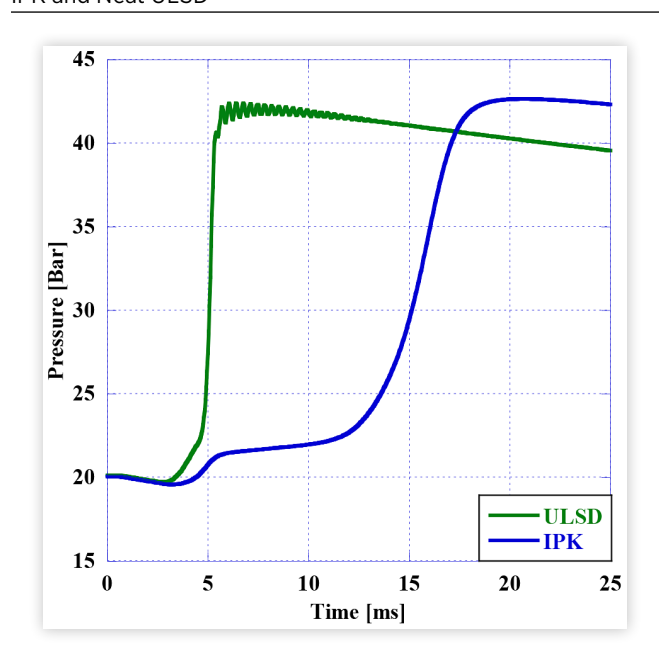
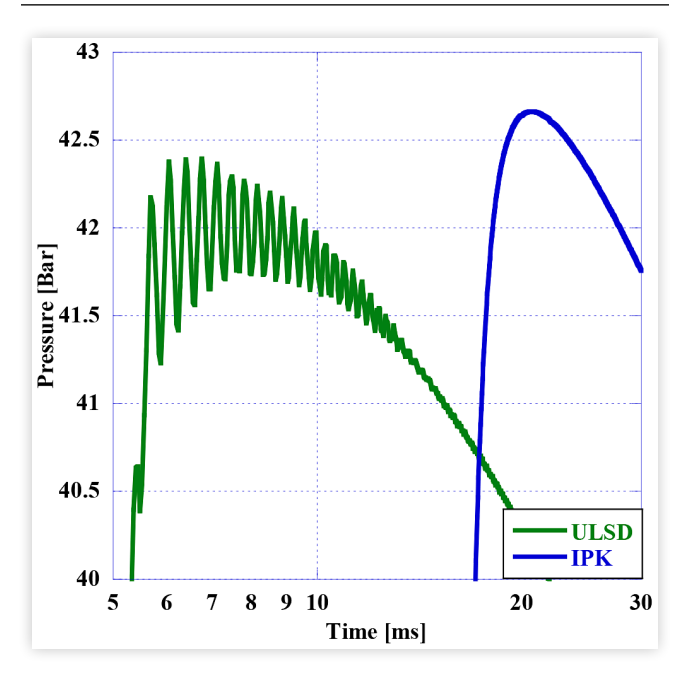
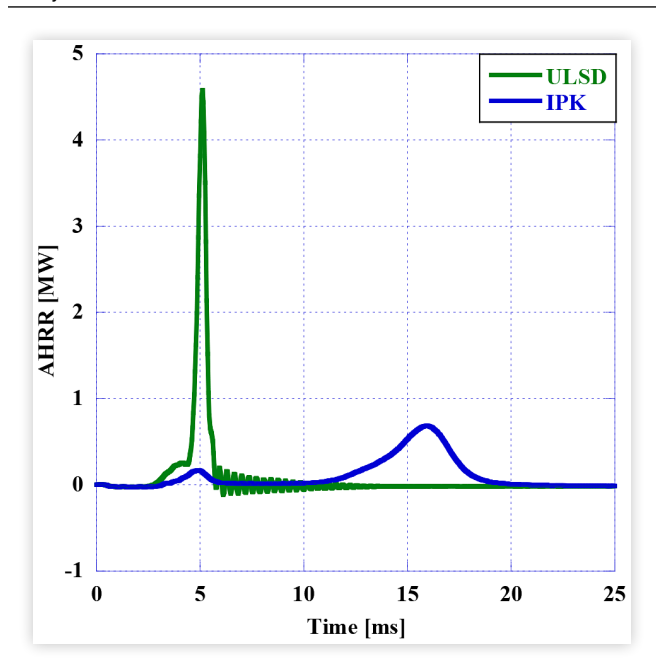


FIGURE 7 Peak Pressures for Neat IPK and ULSD on a Logarithmic Time Scale



that ULSD has clear pressure oscillations at its peak. Alternatively, IPK displays almost no oscillations at all, which is likely due to its higher ignition and combustion delay, and its lower DCN. Additionally, as shown in the apparent heat release rate (AHRR) curves in <u>Fig. 8</u>, IPK has a longer AHRR than diesel, further contributing to reduced oscillations as energy is released at a less abrupt rate [43].

FIGURE 8 AHRR for Neat ULSD and Neat IPK from start of injection



The peak pressures of both ULSD and the time it takes to reach the peaks are listed below in <u>Table 6</u>. This time is measured from the start of injection to the peak pressure. The table displays IPK's slight pressure increase as well as its significant ignition and combustion delay contributing to a later peak pressure time.

TABLE 6 Peak Pressures for Neat IPK and ULSD

Researched Fuel	IPK	ULSD
Time [ms]	20.52	6.76
Peak Pressure [Bar]	42.66	42.40

In addition to analyzing ringing intensity, the recorded pressure traces can provide further insight into the physical and chemical delays of the overall ignition delay. The physical ignition delay is defined as the duration required for the fuel to undergo heating, atomization, vaporization, and mixing. These processes are dependent on the thermophysical properties of the fuel.

The chemical ignition delay occurs following the physical ignition delay, and is influenced by the chemical composition and properties of the fuel. It is the period between chemical decomposition and the onset of rapid reactions leading to combustion, and the time required for the completion of pre-flame reactions that must occur before combustion [44, 45].

Apparent Heat Release Rate and Low Temperature Heat Release in the CVCC

The apparent heat release rate (AHRR) is defined as the usable energy produced by a fuel's combustion. In constant volume combustion analysis, it is a measure of the amount of energy remaining in the combustion chamber to raise the temperature during combustion. AHRR is also used to differentiate between regions of combustion and can be determined from the pressure during combustion.

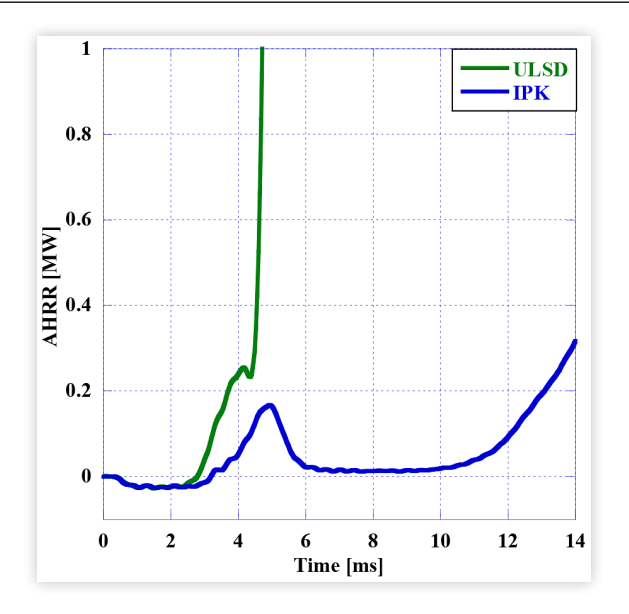
The CVCC is modeled as a closed loop system, heat transfer is neglected, and the wall temperature is assumed to stay at 595.5°C for the duration of combustion. Additionally, combustion is assumed to begin 0.04 ms after injection and the global specific heat ratio is assumed to stay equivalent across all 15 cycles. The equation used to calculated apparent heat release rate can be found below in Equation 3 with a gamma value of 1.4 [46, 47].

$$\frac{dQ}{dt} = \frac{1}{\gamma - 1} V \frac{dP}{dt} \tag{3}$$

The AHRR is plotted as a function of time below in Fig. 8. Comparing the AHRR of IPK to ULSD, it can be seen that ULSD releases heat at a higher rate than IPK does. Despite having more favorable thermophysical properties for combustion than ULSD, such as high volatility and smaller spray atomization, IPK has a much slower combustion period. IPK is observed to reach peak AHRR at around 16 ms, a much longer delay than ULSD which reaches a peak AHRR at around 5 ms.

The apparent heat release rate is also used to investigate the low temperature heat release (LTHR) region. The LTHR of the research fuels are shown below in Fig. 9 by expanding the AHRR plot on the region. Visible for both fuels, but especially IPK, is the spray vaporization between 1 and 3 ms. LTHR is comprised of two sections: the cool flames formation region and the negative temperature coefficient region (NTCR). The first phase of LTHR, the cool flames formation region, begins when AHRR first reaches a non-negative value and continues until it reaches its first peak. Immediately after is the NTC region, which continues until LTHR ends, when AHRR reaches a local minimum. Once AHRR begins to increase, LTHR ends and HTHR begins.

FIGURE 9 LTHR Regions for ULSD and IPK from start of injection



LTHR is the first stage of combustion in which a few main reactions are prevalent: the abstraction of the H atom from fuel molecules, the addition of alkyl radicals to molecular oxygen, and the reactions of the alkylperoxy radicals. These reactions take place are relatively low temperatures and are prevalent here due to their low activation energies [48, 49, 50]. Additionally, these reactions result in the low-luminosity blue flames characteristic of the cool flame formation region, which causes an increase in AHRR. By expanding the duration of LTHR, it is suggested that lower emissions can be achieved [51, 52, 53].

After a peak in LTHR, AHRR begins to decrease despite the increasing temperatures. This is known as the Negative Temperature Coefficient Region (NTCR). NTCR is partially caused by the formation of compounds and radicals that are either stable at low temperatures or absorb more energy in their formation than produced by their combustion. For instance, the formation of ketohydroperoxides, which absorbs more energy in its formation than produced in its combustion, and the HO_2 radical, which is stable at NTCR temperature ranges, both act as an inhibitor for heat release and the formation of other compounds $[\underline{48},\underline{54}]$.

The exact start and end of the NTC region has been a topic of discussion for years, with some sources defining it as the region between LTHR and HTHR, others define an Intermediate Temperature Heat Release between LTHR and HTHR in which NTC lies, and still others define NTC as the decrease in AHRR that occurs between LTHR and HTHR [54, 55]. This paper defines NTCR by the decrease in AHRR between LTHR and HTHR.

Fig. 10 shows the labeled cool flames formation and NTC regions of both researched fuels, which make up LTHR, in an expanded view of Fig. 9. IPK is shown to have a slightly shorter cool flames formation region relative to total combustion time, but a significantly longer NTC region when compared to ULSD. These extended LTHR and NTC regions that IPK has compared to ULSD are correlated with improved emissions quality [47, 56].

Detailed in the tables below are the durations of and amount of energy released by each combustion region. The combustion duration, as defined in this paper, is the time from start of ignition, which begins when AHRR first becomes positive, to end of combustion (EOC), which is when AHRR first falls negative after the main combustion event. It was observed that IPK had a significantly longer duration of all investigated combustion phases than ULSD, a difference of at least 77% in every case. While IPK displayed a significantly longer combustion duration in all investigated regions, it was noted that the energy content between the fuels was much more comparable. ULSD produced approximately 5% more energy in LTHR than IPK, while IPK produced approximately 5% more energy in HTHR. However, when investigating the NTC region, a much larger difference was observed. IPK displayed a 65% increase in energy when compared to ULSD.

FIGURE 10 LTHR Regions for ULSD and IPK from start of injection

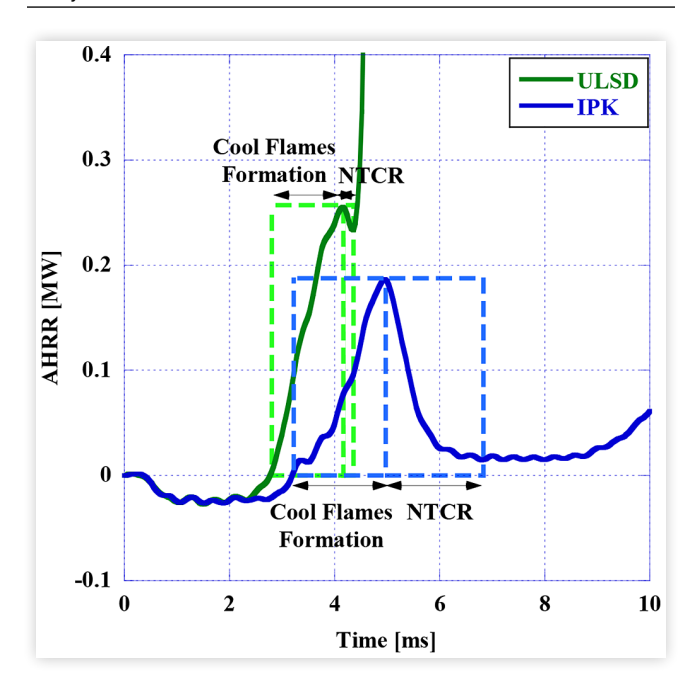


TABLE 7 Energy Released per Combustion Region for ULSD vs. IPK

Researched Fuel	NTCR [J]	LTHR [J]	HTHR [J]
IPK	339.90	469.98	2258.79
ULSD	79.24	264.36	2332.54
% Difference	124.4 %	+56.0 %	-3.2 %

TABLE 8 Duration per Combustion Region for ULSD vs. IPK

Researched Fuel	NTCR [ms]	LTHR [ms]	HTHR [ms]
IPK	7.80	9.52	7.84
ULSD	0.28	1.60	1.28
% Difference	+186.1 %	+142.5 %	+143.9 %

Combustion Characteristics in a Common Rail Direct Injection Experimental Engine

The fired engine testing was conducted using an instrumented experimental diesel engine equipped with a computer-controlled common rail direct injection system. A Kistler 6053cc piezoelectric pressure transducer and Kistler 5010B amplifier were used to collect in-cylinder pressure data, while an Omron E6C3-CWZ3EH rotary encoder was used to capture the rotation of the crankshaft. A schematic of the instrumented head is provided (Fig. 11). Data collection was performed using a Yokogawa DL850 data acquisition system.

The common rail was pressurized by an externally powered Bosch CP3 high pressure radial pump. A Bosch piezoelectric injector was fitted to the engine with a custom machined nozzle to work with the OEM combustion chamber. The injector spray pattern is asymmetric, with the angle reducing from 85° to 50°. A National Instruments DI Driver and Port PFI Driver were interfaced through NI Compact Rio to control the rail pressure, injection timing, number of injections, and engine RPM through closed loop PID control. Intake air flow rates were measured with a Meriam Z50MC-2

FIGURE 11 The instrumented cylinder head

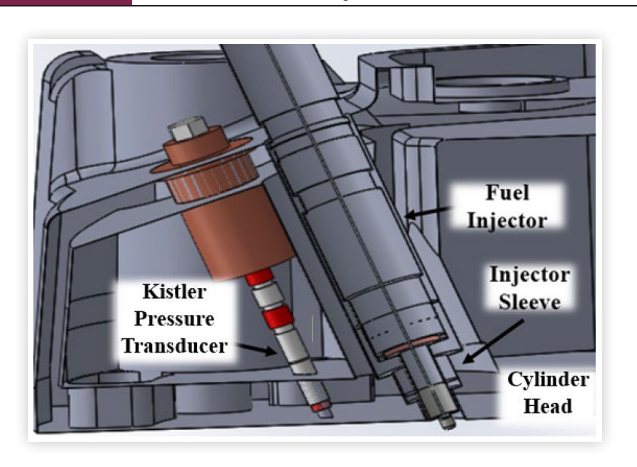


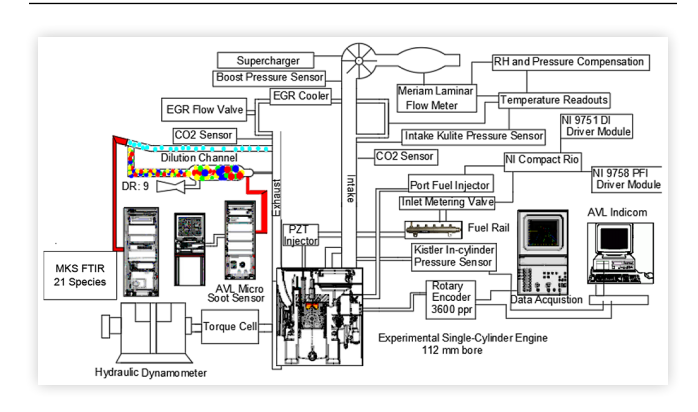
TABLE 9 Specifications of the CRDI Research Engine

<u>Parameter</u>	<u>Value</u>
Peak Power	17kW @ 2200RPM
Peak Torque	77.5 Nm @ 1400 RPM
Bore X Stroke	112 mm x 115 mm
Displacement	1.1L
Number of Cylinders	1
Valves per Cylinder	2
Compression Ratio	16:1
Number of Strokes	4
Injector Nozzle	7x 0.115 mm
Direct Injection System	Common Rail
Direct Injection Pressure	800 bar
Coolant	Water

laminar flow meter. The electronic measurement system interfaced to this unit accounted for the atmospheric conditions.

Realtime analysis of the engine's performance was performed with AVL Indicom software. This allowed for evaluation of the engine's combustion performance including monitoring the combustion phasing (CA50), the Coefficient of Variation (COV), and Pressure rise rate (PRR). A hydraulic dynamometer coupled to the engine's crankshaft was used to apply a load to the engine (measuring brake torque using an Omega TQ513 torque cell). A schematic of the components of the research engine including emissions equipment is provided below (Fig. 12). The engine specifications are presented below in Table 10.

FIGURE 12 Experimental Engine Instrumentation and Equipment



For this experimental research, the engine was operated naturally aspirated in conventional diesel combustion (CDC) at 1500 RPM with a constant load of 4 bar Indicated Mean Effective Pressure (IMEP). The fuel was injected in a single pulse, with the Start of Injection (SOI) being varied for each test point. A total of seven test points were conducted: IPK at 15°, 20°, and 25° SOI, and ULSD at 10.8°, 15°, 16°, and 20° SOI. These timings for IPK were chosen to keep CA50, CoV, and PRR within acceptable limits for this engine. Timing for ULSD test points was adjusted to match CA50 with two of the IPK test points, as well as matching injection timing with IPK at two test points. ULSD was not injected at 25° in order to

keep CA50 within acceptable limits. The summary of test points is provided in <u>Table 10</u> below.

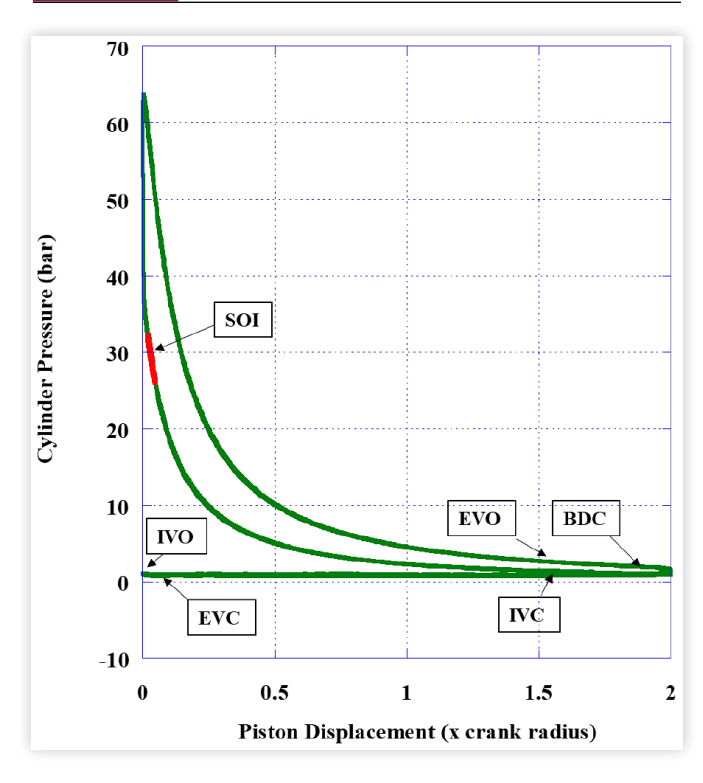
TABLE 10 Injection Parameters (Rail Pressure 800 bar, load 4 bar IMEP)

Fuel	Injection Timing (°BTDC / CAD)	Injection Timing (CAD)	Injection Duration (CAD)	CA50 (ATDC) (CAD)
ULSD	10.8 / 349.2	10.8	5.70	3.72
ULSD	15 / 345	15.0	6.48	2.38
ULSD	16 / 344	16.0	6.41	0.37
ULSD	20 / 340	20.0	6.20	-5.34
IPK	15 / 345	15.0	6.79	10.87
IPK	20 / 340	20.0	6.19	4.86
IPK	25 / 335	25.0	6.51	0.34

Combustion Pressure and Ringing Analysis in the CRDI Engine

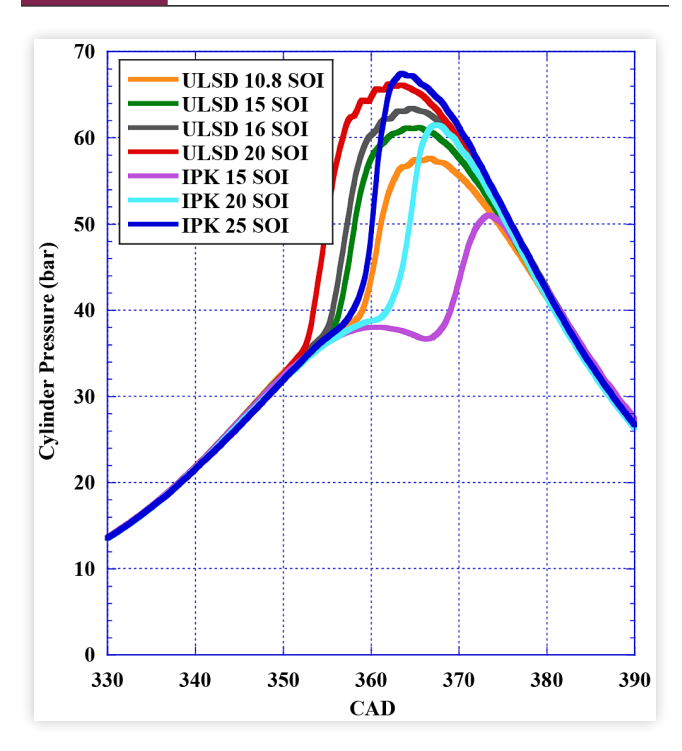
A P-V diagram is given below in <u>Fig. 13</u>, with the injection and valve timings indicated. The piston displacement is given in terms of the crankshaft radius, where TDC equates to 0 displacement, and BDC equates 2x the crank radius. Pressure is given in bar.

FIGURE 13 P-V diagram with injection timing



Combustion pressure is illustrated below in Fig. 14. Here, the effect of advancing injection timing is evident, as peak combustion pressure advances closer to TDC with advancing injection timing. Additionally, the maximum pressure was

FIGURE 14 Combustion Pressure for All Test Points



observed to increase with advancing injection timing. For IPK at 15° and 20° SOI, the peak pressure was observed well after TDC before rapidly rising as IPK combustion completed. At 15° SOI for IPK, the cylinder pressure was observed to reduce after TDC before rising to the peak pressure. The long ID and CD of IPK cause this delay in combustion until significantly after TDC. However, with the advance of injection timing, the peak pressure location was shifted closer to TDC, more closely matching the trends of ULSD. When matching injection timing for IPK and ULSD, peak combustion pressure was delayed by 16.6% and 7.2% for 15° BTDC SOI and 20° BTDC SOI, respectively.

Results for peak pressure analysis are given in <u>Table 11</u>. When comparing the researched fuels at matched injection timings, IPK exhibited lower peak pressures that occurred significantly farther after Top Dead Center (TDC) than ULSD. The Pressure Rise Rate (PRR) refers to the rate at which pressure increased in bar per crank angle degree (CAD).

TABLE 11 Peak Pressure and Ringing during combustion

Fuel	Injection Timing (°BTDC / CAD)	Peak Pressure (bar)	Peak Pressure Location (CAD)	Pressure rise rate (bar/ CAD)	Ringing Intensity (MW/ m²)
ULSD	10.8 / 349.2	57.62	366.72	6.22	1.49
ULSD	15 / 345	61.19	365.46	6.64	1.44
ULSD	16 / 344	63.41	364.74	6.47	1.92
ULSD	20 / 340	66.24	362.22	7.75	1.98
IPK	15 / 345	51.02	373.38	3.96	0.43
IPK	20 / 340	61.48	367.26	7.83	1.48
IPK	25 / 335	67.47	363.48	11.37	3.22

Higher PRR indicates more rapid combustion rate and faster combustion progression throughout the combustion chamber as the diffusion flame at each injector spray mixes with air [57]. With IPK, this occurs when the injection timing is advanced such that the physical and chemical ignition delays have had time to occur, allowing a more homogeneous mixture to be produced throughout the cylinder, with combustion beginning as the piston is still in the compression stroke [36]. This is evident as injection timing increased for IPK, PRR increased from 3.54 bar/CAD at 15° BTDC SOI to 10.28 bar/CAD at 25° BTDC SOI. The chemical ignition delay inherent in IPK due to the low ratio of n-paraffin to isoparaffin content [11, 58, 59] is mitigated by the advanced injection timing. Therefore, as timing was advanced to 20° and beyond, due to the high volatility and ability to form a homogenous air/fuel mixture within the combustion chamber before autoignition, IPK exhibited a greater PRR.

When comparing the fuels at matched combustion phasing (CA50), ULSD was injected at 10.8° BTDC to match with IPK at 20° BTDC, and at 16° BTDC to match with IPK at 25° BTDC. In both matched CA50 cases, the peak pressure location aligned closely between ULSD and IPK; however, the peak pressure was significantly higher for IPK when compared to ULSD. PRR for IPK was also higher when combustion phasing was matched.

Also given in <u>Table 11</u> is the Ringing Intensity (RI) for each of the test points. Ringing intensity was determined with <u>Equation 5</u> using peak pressure, PRR, and peak temperature. The constant β was set at 0.05 determined from literature [60]. Ringing intensity is seen to increase with advancing injection timing. When matching injection timing, IPK exhibits lower ringing intensity than ULSD. However, when matching combustion phasing with ULSD, RI for IPK increases rapidly with advancing injection timing.

$$RI = \frac{\left(\beta \left(\frac{dP}{dt}\right)_{max}\right)^{2}}{\left(2\gamma P_{max}\right)} \sqrt{\gamma R T_{max}}$$
 (5)

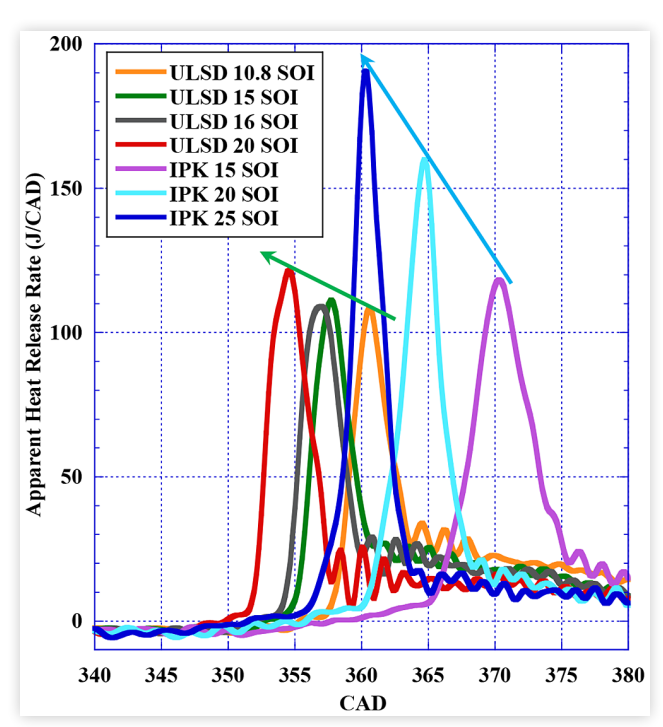
Apparent Heat Release Rate and Low Temperature Heat Release in the CRDI Engine

The AHRR was obtained from the measured combustion pressure using the model in <u>Equation 6</u>. This model applies the first law of thermodynamics to a closed system with a homogeneous mixture operating under the ideal gas law during the compression and expansion strokes.

$$\frac{dQ}{d\theta} = \frac{1}{(\gamma - 1)} V \frac{dP}{d\theta} + \frac{\gamma}{(\gamma - 1)} P \frac{dV}{d\theta}$$
 (6)

The full apparent heat release rate plot encompassing injection and main combustion events for all test points is provided below (Fig. 15).





IPK is observed to have a sharper rise in AHRR compared to ULSD, particularly at advanced injection timings. This is correlated with the PRR and RI analysis, where advancing injection timing allows for mitigation of the chemical delay resulting in rapid heat release from the combustion event. With the earlier injection timing, the energy drop due to the vaporization of the fuel occurs earlier in the compression stroke. This allows more time for the air/fuel charge to reach a combustible mixing before the piston reaches TDC [61]. The higher temperature and pressure of the mixture resulted in a shorter chemical ignition delay and a more rapid combustion [22]. Additionally, IPK's peak AHRR was significantly higher than that for ULSD when matching injection timings.

The values for peak AHRR and peak AHRR location, CA50, and CoV are provided in <u>Table 12</u> below. When matching CA50 at 360.4° (ULSD at 16° SOI and IPK at 25° SOI), the peak heat release rate for IPK was 74.7% greater than

TABLE 12 Peak AHRR, CA50, and CoV during combustion

Fuel	Injection Timing (°BTDC / CAD)	Peak Heat Release Rate (J/ CAD)	Peak Heat Release Rate Location (CAD)	CA50 (ATDC) (CAD)	CoV (%)
ULSD	10.8 / 349.2	108.37	360.60	3.72	3.18
ULSD	15 / 345	111.20	357.72	2.38	2.57
ULSD	16 / 344	109.08	357.00	0.37	2.80
ULSD	20 / 340	121.56	354.66	-5.34	2.95
IPK	15 / 45	118.23	370.32	10.87	2.15
IPK	20 / 340	159.86	364.74	4.86	2.21
IPK	25 / 335	190.54	360.24	0.34	2.10

ULSD. However, Peak AHRR location was 357° for ULSD and 360.24 for IPK. This was also observed when matching combustion phasing near 364°, where ULSD again had a lower peak heat release rate, but the location of peak AHRR was advanced compared to IPK.

Furthermore, for IPK, CA50 was observed to closely follow the location of peak heat release, with a deviation of less than 0.60° CAD. This trend was not observed with ULSD, where CA50 consistently occurred several CAD after the location of peak heat release rate.

Examining only the LTHR region of combustion, significant variation in the duration of LTHR is observed. Furthermore, IPK exhibited extended duration in LTHR due to the thermophysical properties and long ID and CD as found in the CVCC.

For a clearer analysis of the LTHR of the researched fuels, AHRR plots of ULSD at 16° SOI and IPK at 25° SOI, as well as ULSD at 20° SOI and IPK at 20° SOI are presented below (Fig. 16 and Fig. 17). In these figures, a defined decrease in the AHRR is seen to coincide with SOI, followed by oscillations in AHRR as the in-cylinder pressure sensor is buffeted by pressure waves from the injection event.

After the injection event is completed, a distinct decrease in AHRR is observed coinciding with the physical ignition delay as the vaporizing fuel droplets are dispersed through the combustion chamber, absorbing heat from the cylinder walls and compressed air charge [57]. As the mixing fuel/air charge continues to compress, the AHRR reaches a point of inflection signifying the end of the physical ignition delay and the start of the chemical ignition delay. At this point, AHRR begins to rise as the chemical ignition delay and exothermic

FIGURE 16 LTHR of ULSD at 20° SOI and IPK at 20° SOI (matched injection timing)

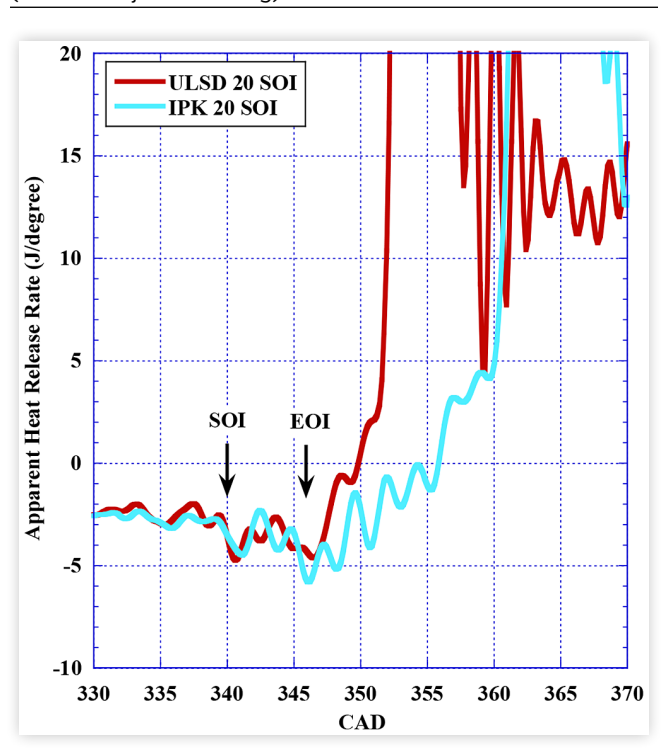
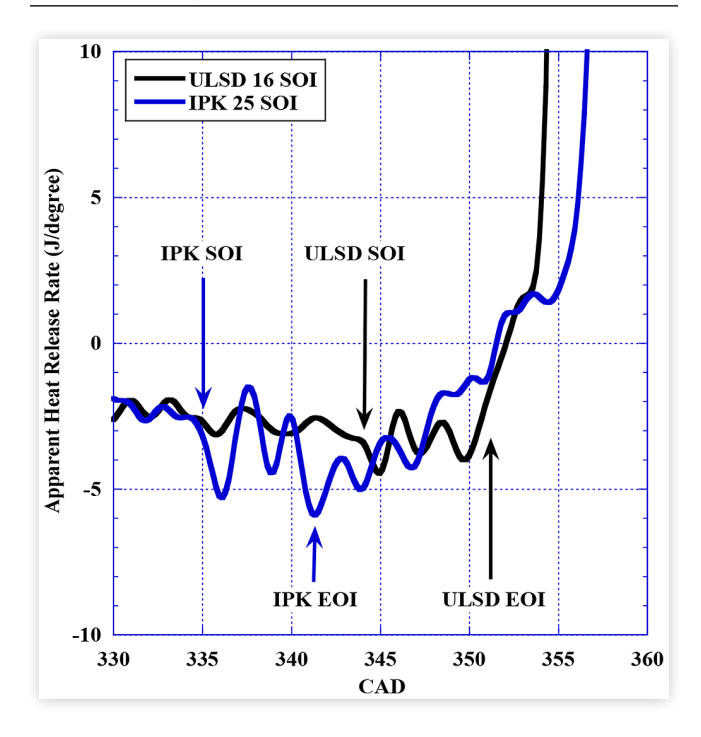


FIGURE 17 LTHR of ULSD at 16° SOI and IPK at 25° SOI (CA50 matched)



reactions take place [62, 63]. Similar to the combustion regions as defined in the CVCC, when the AHRR becomes positive in value, the cool flame formation of LTHR has begun. Following a peak in cool flame formation, a decrease in AHRR is exhibited by the NTC region. When the AHRR again reaches the value of the first peak during cool flame formation, High Temperature Heat Release (HTHR) begins.

For IPK at all injection timings, there are a greater number of oscillations after the injection event in NTC region, suggesting that multiple jets reach the LTHR and NTCR sequentially. The geometry of the piston bowl and injector nozzle is such that the sprays encounter air with differing temperature and turbulence profiles, resulting in some sprays beginning premixed burn earlier than others. This is observed as oscillations in the AHRR calculated from the pressure trace as the in-cylinder pressure transducer is buffeted by shockwaves from the localized combustion events. Upward trends in AHRR represent the formation of cool flames releasing energy, while the downward trends in AHRR represent a slowing in the combustion process as energy is predominantly absorbed by the vaporization and mixing of the fuel. This oscillating phenomenon is not as pronounced with ULSD (Fig. 16 Fig. 17), due to its slower atomization and vaporization qualities, which result in delayed formation of combustible A/F ratio pockets and fewer oscillations in AHRR before the premixed combustion event. However, due to the overall decreased ID for ULSD, the bulk premixed combustion event occurs sooner than for IPK.

When injection timing was matched between ULSD and IPK (Fig. 17), IPK's extended physical and chemical ignition delay is clearly observable, as well as the extended duration in LTHR compared to ULSD. When CA50 was matched with ULSD at 16° BTDC SOI and IPK at 25° BTDC SOI, the LTHR

region in Fig. 17 clearly reveals the greater ignition delay of IPK.

Emissions Analysis

An analysis was conducted on the emissions produced by the engine at each of the test points with both researched fuels. Results of this analysis provide critical insight into the viability of alternative fuels for reducing greenhouse gas pollution. Furthermore, these emissions results allow for a more complete understanding of the combustion characteristics of the F-T fuel IPK in a CI engine. Emissions analysis was conducted using a 21 species MKS FTIR for measurement of NO_{x} , CO , CO_{2} , and Unburned Hydrocarbons (UHC). Soot was measured using an AVL 415s Smoke Meter.

It is seen in Fig. 18 that $\mathrm{NO_x}$ was reduced with IPK when matching injection timing. However, when matching CA50 with ULSD, greater concentration of $\mathrm{NO_x}$ was observed with IPK at the same load. This is due to the higher temperatures associated with combustion at the higher pressures that IPK exhibited when matching CA50 with diesel. This is also responsible for the general trend across all test points as injection timing was advanced, more NOx was produced, which is supported by literature [64]. Soot emissions are seen to decrease with IPK compared to ULSD (Fig. 19). When matching CA50, soot was particularly reduced with IPK.

The tradeoff plot of NO_x vs Soot emissions is presented below <u>Fig. 20</u>. NO_x is seen to increase with advancing injection timing while soot emissions are observed to decrease.

 CO_2 emissions for IPK were slightly reduced at 20° SOI when matching either injection timing or CA50 with ULSD. However, at further advanced timing of 25° SOI, IPK produced more CO_2 compared to ULSD at matched CA50. When matching injection timing at 15° SOI, IPK produced slightly more CO_2 than ULSD (Fig. 21).



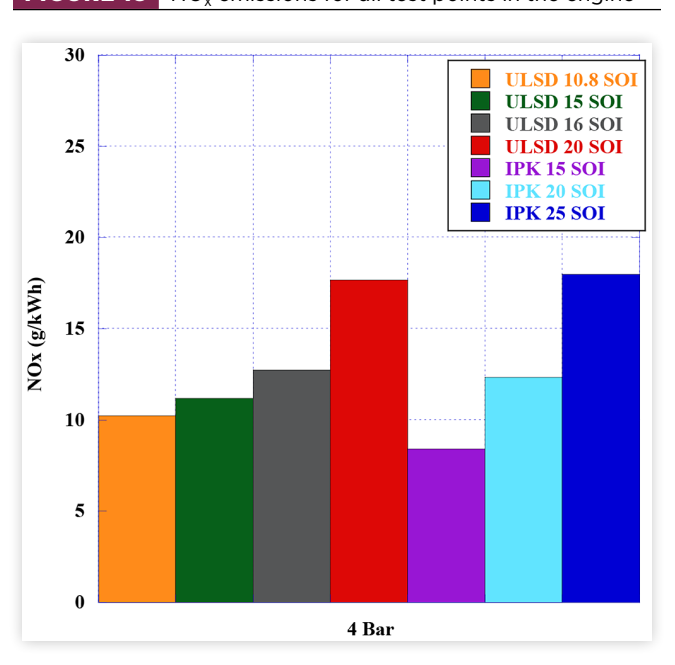


FIGURE 19 Soot emissions for all test points in the engine

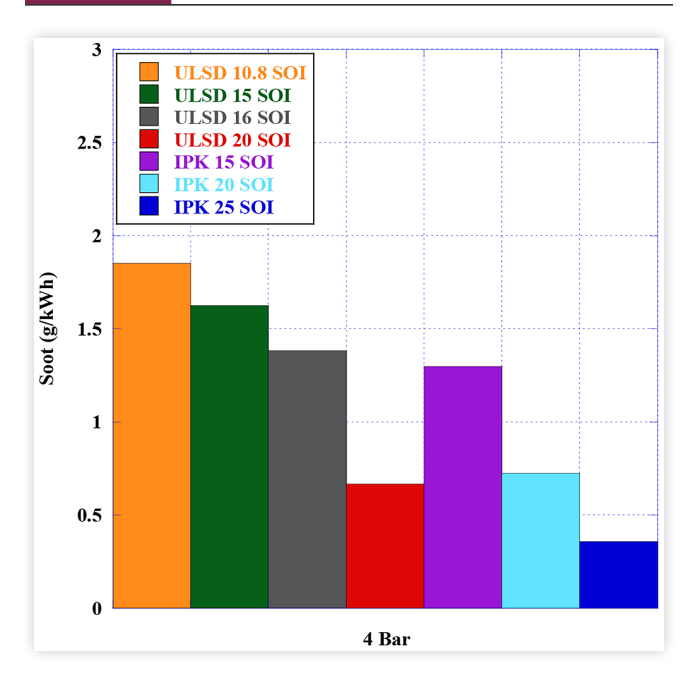
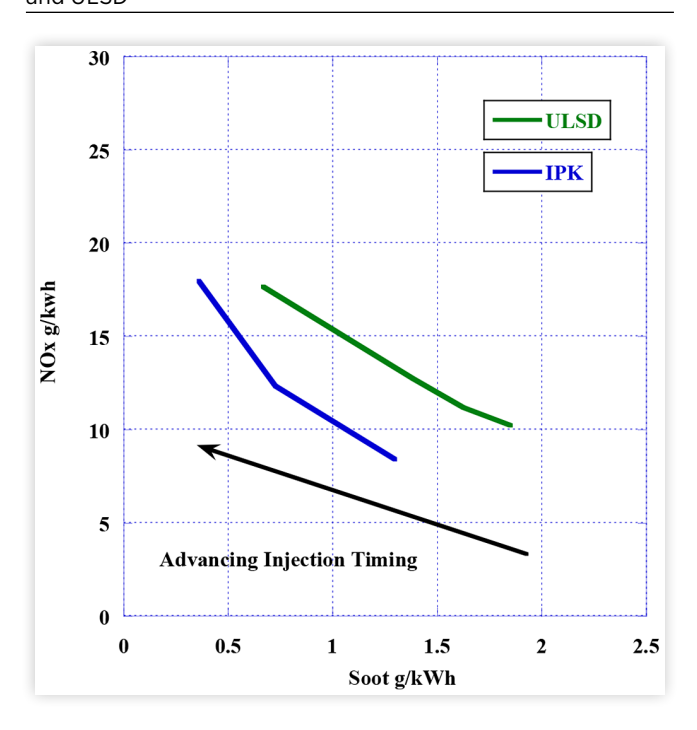


FIGURE 20 Tradeoff NOx versus Soot Emissions for IPK and ULSD



Emissions of CO were significantly increased for IPK across all injection timings (<u>Fig. 22</u>). Furthermore, for both ULSD and IPK, a reduction in CO emissions is seen with advancing injection timing. The greatest reduction in CO is observed when advancing timing such that peak pressure occurred above 61 bar, which occurs for ULSD at 15° SOI and for IPK at 20° SOI.

The UHC emissions from the engine are provided below in <u>Fig. 23</u>. IPK is seen to produce more UHC than ULSD across all test points. Correlating with UHC emissions, combustion



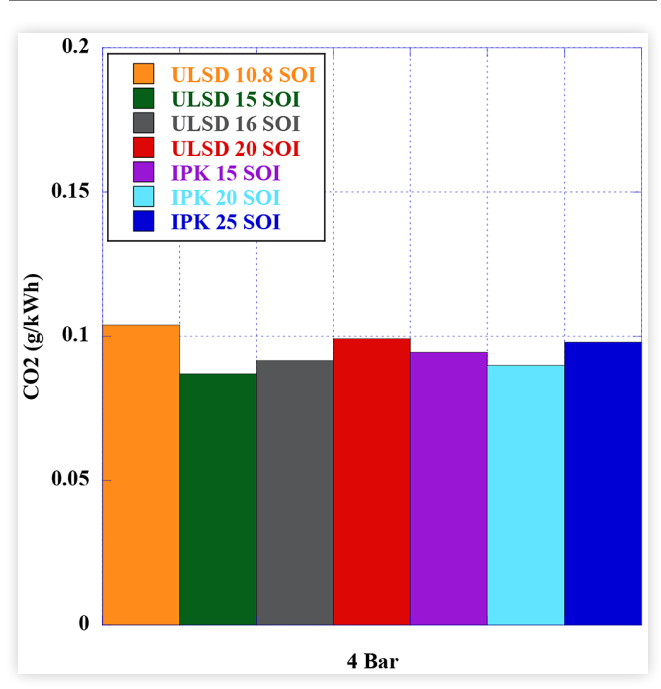
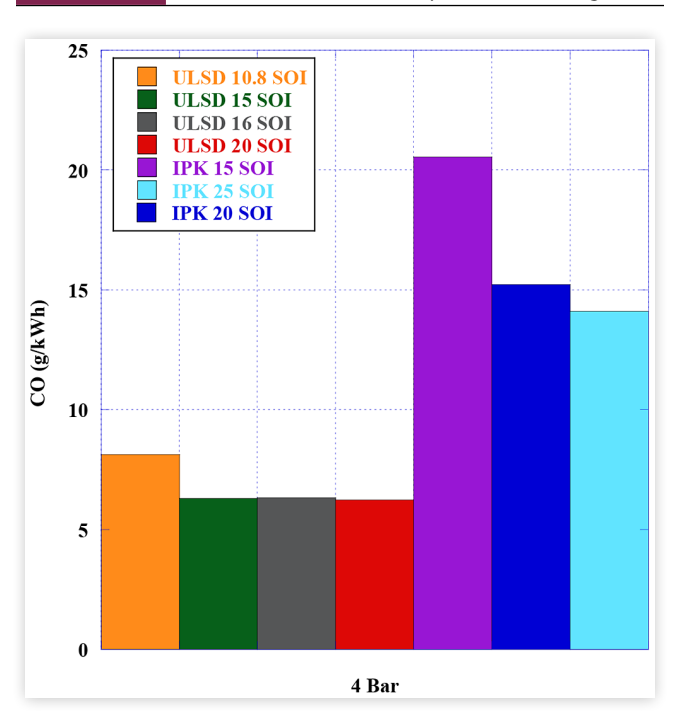


FIGURE 22 CO emissions for all test points in the engine



efficiency is an indication of how completely the fuel was combusted in the engine (<u>Fig. 24</u>). Combustion efficiency was calculated using <u>Equation 7</u> where the energy carried out of the engine by the mass fraction of combustible species (x_i) is compared to the total energy content of the fuel. The subscripts a and f denote air and fuel, respectively, while Q_{HV} refers to the lower heating value of the species. Accepted heating values for CO and H_2 of 10.1 MJ/kg and 120 MJ/kg were used, respectively. The fuel heating value was used for the unburned hydrocarbon composition [<u>57</u>].

FIGURE 23 Unburned Hydrocarbons for all test points in the engine

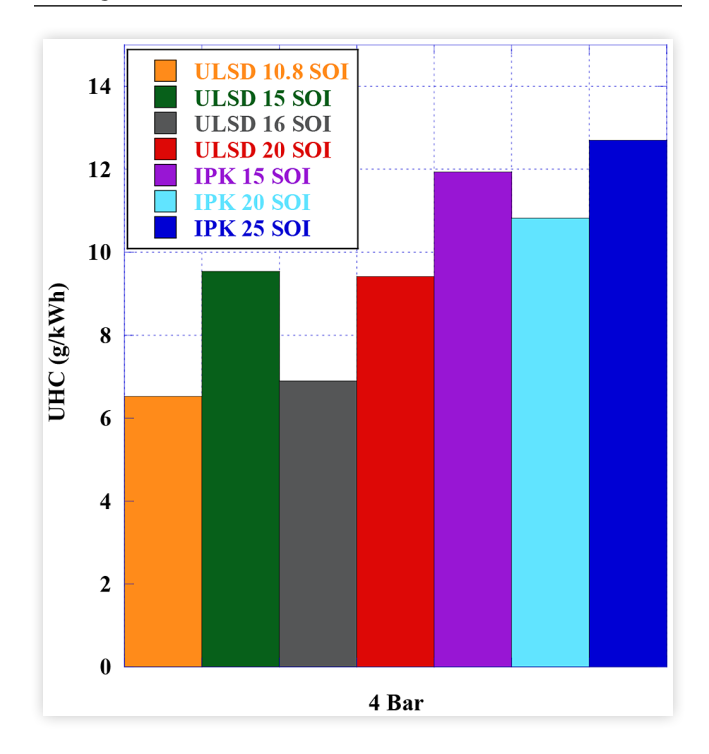
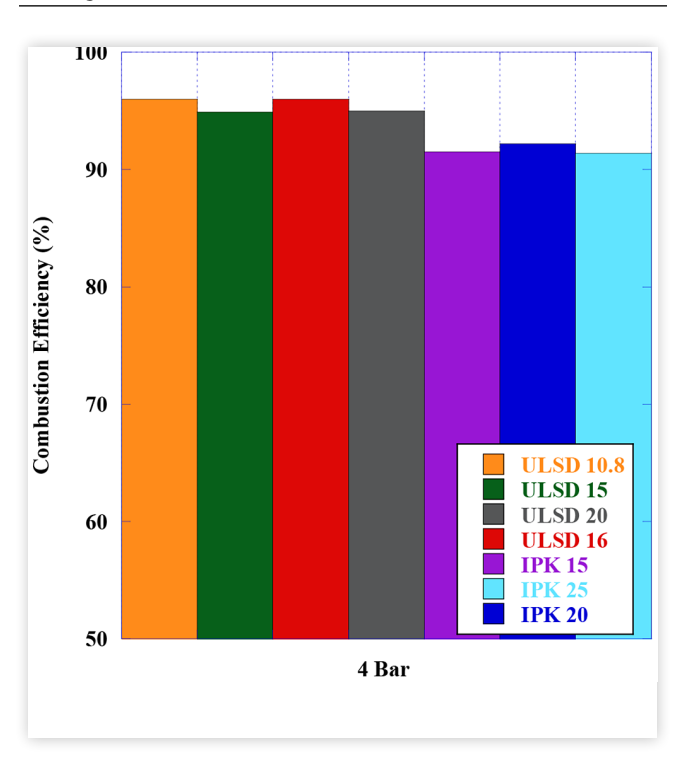
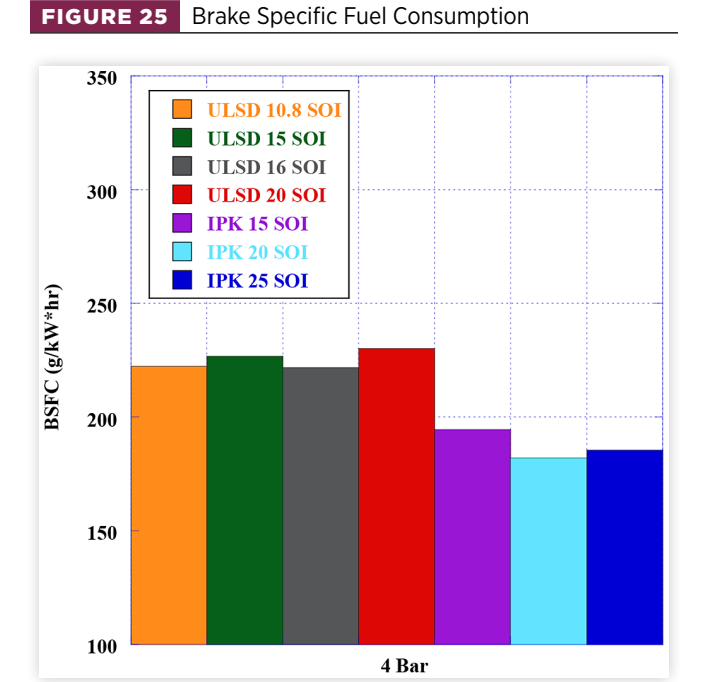


FIGURE 24 Combustion efficiency for all test points in the engine



$$\eta_c = 1 - \frac{\sum_i x_i Q_{HV}}{\left[\frac{\dot{m}_f}{\dot{m}_a + \dot{m}_f}\right]} Q_{HV_f}$$
(7)



For IPK, the combustion efficiency was between 91.5% and 92.5%, while ULSD's combustion efficiency was higher at 95-96%, indicating more complete combustion due to the combustion chamber geometry and the physical and chemical properties of the fuel.

The Brake Specific Fuel Consumption (BSFC) was calculated <u>Fig. 25</u>, taking into account the different densities of the fuels. At the constant load of 4 bar IMEP, IPK exhibited a reduction in BSFC for all injection timings, favoring 20° SOI.

Summary/Conclusions

The Fischer-Tropsch CTL fuel IPK was researched for potential applications in CI engines with modified injection strategy. Several analyses were conducted in the laboratory to investigate each fuel's thermophysical properties and combustion characteristics before the fuel was investigated in a CRDI single-cylinder research engine. Physical and chemical ignition delay, combustion delay, apparent heat release rate, combustion pressure, pressure rise rate, fuel consumption, and 21 species emissions and soot were evaluated at a constant load of 4 bar IMEP, with variable timing of a single injection pulse.

Analyzing the thermophysical properties of the fuels revealed that IPK's low viscosity and density gives it distinctly favorable spray atomization quality which enhances droplet distribution and mixture formation. This combined with IPK's high volatility results in a reduced physical ignition delay in the engine compared to ULSD. The chemical ignition delay was found to be longer for IPK due to the chemical properties of IPK that require more time to begin exothermic reactions in the combustion chamber. Specifically, the low ratio of n-paraffins to iso-paraffins and high concentration of branched chain alkanes resist auto ignition and together with

the very low DCN of approximately 26, cause this extended ignition delay.

For two test points per fuel, injection timing was matched between IPK and ULSD at 15° BTDC SOI and 20° BTDC SOI.

- Peak combustion pressure was delayed significantly for IPK when matching injection timing. This is due to the long ignition delay experienced by IPK which requires more time for combustion to occur. Pressure rise rate was lower for IPK at 15° SOI compared to ULSD at 15° SOI, but as timing was advanced to 20° and beyond, IPK exhibited a greater PRR due to high volatility and ability to form a highly homogenous air/fuel mixture within the combustion Ringing intensity was less for IPK than ULSD when matching injection timing.
- AHRR for IPK was greater than ULSD when matching injection timing, however due to the long ignition delay as supported by research in the CVCC, peak AHRR for IPK is later than ULSD.
- In emissions analysis, IPK at matched timing with ULSD produced less NO_x, and at 20° exhibited in soot and CO₂. For all injection timings studied, CO and UHC increased with IPK compared to ULSD. BSFC was reduced for IPK in all cases.

For two test points per fuel, injection timing was adjusted to match CA50 with IPK and ULSD in the following cases: ULSD at 10.8° BTDC SOI and IPK at 20° BTDC SOI; and ULSD at 16° BTDC SOI and IPK at 25° BTDC SOI.

- Peak combustion pressure for IPK occurred much closer to ULSD peak pressure when matching combustion phasing. Because the fuel charge had more time in the combustion chamber before ignition, the extended ignition delay of IPK was mitigated. However, ringing intensity was observed to increase with increasing injection timing for IPK.
- AHRR for IPK was also greater than ULSD when matching CA50. Additionally, the location of peak AHRR followed very closely the location of CA50 for IPK, a trend not observed with ULSD.
- In emissions analysis, IPK matched CA50 with ULSD produced more NO_x. However, soot was significantly reduced compared to ULSD at the same combustion phasing. CO₂ was reduced for IPK at 20° BTDC SOI compared to ULSD at 10.8° BTDC SOI.

For all injection timings studied, IPK exhibited more oscillations in the AHRR curve before the LTHR region compared to ULSD. This is due to the chemical reactions that take place during the chemical ignition delay stage before the AHRR increases above 0. Furthermore, during LTHR combustion, IPK exhibited two regions of cool flame formation and NTCR, which was not observed with ULSD at any injection timing studied.

IPK exhibited more favorable combustion characteristics when the injection timing was advanced compared to the default injection timing for the CRDI research engine platform. The advanced injection timing allowed time for the chemical ignition delay to occur. Some key GHG emissions

were reduced with the use of IPK, including CO_2 , NO_x , and soot at certain injection timings. CO was increased at all injection timings studied. BSFC was reduced with IPK in all cases.

References

- "Synthetic Fuels," https://www.sciencedirect.com/topics/engineering/synthetic-fuel.
- "Synthetic Fuels," https://www.sfc.com/en/glossar/synthetic-fuels/.
- Majewski, W.A., "Synthetic Diesel Fuel," https://dieselnet.com/tech/fuel_synthetic.php#f-t.
- Huang, S., Deng, P., Huang, R., Wang, Z. et al., "Visualization Research on Spray Atomization, Evaporation and Combustion Processes of Ethanol–Diesel Blend Under LTC Conditions," *Energy Conversion and Management* 106 (2015): 911-920, https://doi.org/10.1016/j.enconman.2015.10.028.
- Kahandawala, M., DeWitt, M., and Corporan, E., "Ignition and Emissions Characteristics of Surrogate and Practical Jet Fuels," *Energy & Fuels* 22, no. 6 (2008): 3673-3679, https://doi.org/10.1021/ef800303a.
- Corporan, E., DeWitt, M., and Belovich, V., "Emissions Characteristics of a Turbine Engine and Research Combustor Burning Fischer-Tropsch Jet Fuel," *Energy & Fuels* 21, no. 5 (2007): 2615-2626, https://doi.org/10.1021/ef070015j.
- Mofijur, M., Masjuki, H., and Kalam, M., "Effect of Biodiesel from Various Feedstocks on Combustion Characteristics, Engine Durability, and Materials Compatibility: A Review," Renewable and Sustainable Energy Reviews 28 (2013): 441-455, https://doi.org/10.1016/j.rser.2013.07.051.
- 8. Labbe, R., Paczkowski, S., and Knappe, V., "Effect of Feedstock Particle Size Distribution and Feedstock Moisture Content on Pellet Production Efficiency, Pellet Quality, Transport and Combustion Emissions," *Fuel* 263 (2020): 116662, https://doi.org/10.1016/j.fuel.2019.116662.
- Zhang, Y., Guo, Y., and Cheng, F., "Investigation of Combustion Characteristics and Kinetics of Coal Gangue with Different Feedstock Properties by Thermogravimetric Analysis," *Thermochimica Acta* 614 (2015): 137-148, https://doi.org/10.1016/j.tca.2015.06.018.
- 10. "Celebrating Our Heritage," Sasol, https://www.sasol.com/celebrating-our-heritage.
- 11. Hui, X., Kumar, K., and Sung, C.-J., "Experimental Studies on the Combustion Characteristics of Alternative Jet Fuels," *Fuel* 98 (2012): 176-182, https://doi.org/10.1016/j.fuel.2012.03.040.
- 12. Frame, E., Alvarez, R., and Yost, D., "Evaluation of Synthetic Fuel for Army Ground Applications: Tasks 2-6," 2005.
- 13. Schulman, M. and Frame, E., "Engine Durability Evaluation Using Synthetic Fuel in a Catepillar C7 Engine," 2007.
- Qian, Y., Zhang, Y., and Lu, X., "Effects of Different Aromatics Blended with Diesel on Combustion and Emissions Characteristics with a Common Rail Diesel Engine," *Applied Thermal Engineering* 125 (2017): 1530-1538, https://doi.org/10.1016/j.applthermaleng.2017.07.145.

- Hong, F., Alghamdi, N., and Bailey, A., "Chemical and Kinetic Insights into Fuel Lubricity Loss of Low-Sulfur Diesel Upon the Addition of Multiple Oxygenated Compounds," *Tribology International* 152: 106559, https://doi.org/10.1016/j.triboint.2020.106559.
- Joshi, U., Zheng, Z., Shrestha, A., Henein, N. et al., "An Investigation on Sensitivity of Ignition Delay and Activation Energy in Diesel Combustion," *Journal Of Engineering for Gas Turbines and Power* 137 (2014): 091506, https://doi.org/10.1115/1.4029777.
- Kang, D., Bohac, S.V., Boehman, A.L., Cheng, S. et al., "Autoignition Studies of C5 Isomers in a Motored Engine," Combustion Institute 36 (2017): 3597-3604, https://doi. org/10.1016/j.proci.2016.09.012.
- Emberger, P., Hebecker, D., Pickel, P., Remmele, E. et al., "Ignition and Combustion Behaviour of Vegetable Oils After Injection in a Constant Volume Combustion Chamber," *Biomass and Bioenergy* 78 (2015): 48-61, https://doi. org/10.1016/j.biombioe.2015.04.009.
- Jing, W., Wu, Z., Roberts, W.L., and Fang, T., "Spray Combustion of Biomass-Based Renewable Diesel Fuel Using Multiple Injection Strategy in a Constant Volume Combustion Chamber," Fuel 181 (2016): 718-728, https://doi. org/10.1016/j.fuel.2016.05.039.
- Liu, Y., Li, J., and Jin, C., "Fuel Spray and Combustion Characteristics of Butanol Blends in a Constant Volume Combustion Chamber," *Energy Conversion and Management* 105 (2015): 1059-1069, https://doi.org/10.1016/j.enconman.2015.08.047.
- Kang, D., Kalaskar, V., Kim, D., Martz, J. et al., "Experimental Study of Autoignition Characteristics of Jet-A Surrogates and Their Validation in a Motored Engine and a Constant-Volume Combustion Chamber," *Fuel* 184 (2016): 565-580, https://doi.org/10.1016/j.fuel.2016.07.009.
- Soloiu, V., Wiley, J., and Gaubert, R., "Fischer-Tropsch Coalto-Liquid Fuel Negative Temperature Coefficient Region (NTC) and Low-Temperature Heat Release Rate (LTHR) in a Constant Volume Combustion Chamber (CVCC)," *Energy* 198 (2020): 117288, https://doi.org/10.1016/j.energy.2020.117288.
- Soloiu, V., Weaver, A., and Smith, R., "Combustion Characteristics of Low DCN Synthetic Aviation Fuel, IPK, in a High Compression Ignition Indirect Injection Research Engine," SAE Technical Paper <u>2023-01-0272</u> (2022), https://doi.org/10.4271/2023-01-0272.
- Atkinson, C., Thompson, G., and Traver, M., "In-Cylinder Combustion Pressure Characteristics of Fischer-Tropsch and Conventional Diesel Fuels in a Heavy-Duty CI Engine," SAE Technical Paper <u>1999-01-1472</u> (1999), https://doi.org/10.4271/1999-01-1472.
- Tess, M., Kurman, M., and Kweon, C., "Spray Characterization and Ignition Delay Measurements of JP-8 and IPK in a Constant-Pressure Flow Chamber," SAE Int. J. Engines 9, no. 2 (2016): 899-909, https://doi.org/10.4271/2016-01-0736.
- Caton, J., "Combustion Phasing for Maximum Efficiency for Conventional and High Efficiency Engines," *Energy Conversion and Management* 77 (2014): 564-576, https://doi.org/10.1016/j.enconman.2013.09.060.

- Das, P., Subbarao, P., and Subrahmanyam, J., "Effect of Main Injection Timing for Controlling the Combustion Phasing of a Homogeneous Charge Compression Ignition Engine using a New Dual Injection Strategy," *Energy Conversion and Management* 95 (2015): 248-258, https://doi.org/10.1016/j.enconman.2015.02.018.
- Zhang, Z., Liu, H., Yue, Z., Wu, Y. et al., "Effects of Multiple Injection Strategies on Heavy-Duty Diesel Energy Distributions and Emissions Under High Peak Combustion Pressures," Frontiers in Energy Research 10 (2022), https://doi.org/10.3389/fenrg.2022.857077.
- 29. Armas, O., Yehliu, K., and Boehman, A., "Effect of Alternative Fuels on Exhaust Emissions during Diesel Engine operation with Matched Combustion Phasing," *Fuel* 89, no. 2 (2009): 438-456, https://doi.org/10.1016/j.fuel.2009.09.022.
- Dec, J. and Sjolberg, M., "Isolating the Effects of Fuel Chemistry on Combustion Phasing in an HCCI Engine and the Potential of Fuel Stratification for Ignition Control," SAE Technical Paper 2004-01-0557 (2004), https://doi. org/10.4271/2004-01-0557.
- 31. Stafford, J., Amezcua, E., and Narasimhamurthy, M., "Combined Impacts of Engine Speed and Fuel Reactivity on Energy-Assisted Compression-Ignition Operation with Sustainable Aviation Fuels," SAE Technical Paper 2023-01-0263 (2023), https://doi.org/10.4271/2023-01-0263.
- 32. Das, P., Selokar, M., Subbarao, P., and Subrahmanyam, J., "Effect of Injection Timing, Premixed Equivalence Ratio and EGR on Combustion Characteristics of an HCCI-DI Combustion Engine Using In-Cylinder Dual Injection Strategy," SAE Technical Paper 2016-01-0752 (2016), https://doi.org/10.4271/2016-01-0752.
- 33. Jing, W., Roberts, W.L., and Fang, T., "Spray Combustion of Jet-A and Diesel Fuels in a Constant Volume Combustion Chamber," *Energy Conversion and Management* 89 (2015): 525-540, https://doi.org/10.1016/j.enconman.2014.10.010.
- Zeng, W., Sjoberg, M., Reuss, D., and Zongjie, H., "High-Speed PIV, Spray, Combustion Luminosity, and Infrared Fuel-Vapor Imaging for Probing Tumble-Flow-Induced Assymetry of Gasoline Distribution in a Spray-Guided Stratified-Charge Disi Engine," *Proceedings of The Combustion Institute* 36 (2017): 3459-3466, https://doi.org/10.1016/j.proci.2016.08.047.
- Manigandan, S., Gunasekar, P., Poorchilamban, S., and Nithya, S., "Effect of Addition of Hydrogen and TIO2 in Gasoline Engine in Various Exhaust Gas Recirculation Ratio," *International Journal of Hydrogen Energy* 44 (2019): 11205-11218, https://doi.org/10.1016/j.ijhydene.2019.02.179.
- 36. Soloiu, V., Weaver, A., Smith, R., Rowell, A. et al., "Combustion Characteristics of Low DCN Synthetic Aviation Fuel, IPK, in a High Compresion Ignition Indirect Injection Research Engine," SAE Technical Paper <u>2023-01-0272</u> (2023), https://doi.org/10.4271/2023-01-0272.
- Farrell, J.T., Cernansky, N.P., Dryer, F.L., Law, C.K. et al., "Development of an Experimental Database and Kinetic Models for Surrogate Diesel Fuels," SAE Technical Paper 2007-01-0201 (2007), https://doi.org/10.4271/2007-01-0201.
- 38. Zhang, C., Hui, X., Lin, Y., and Sung, C.-J., "Recent Development in Studies of Alternative Jet Fuel Combustion:

- Progress, Challenges, and Opportunities," *Renewable and Sustainable Energy Reviews* 54 (2016): 120-138, https://doi.org/10.1016/j.rser.2015.09.056.
- 39. Opacich, K., Peiffer, E., Heyne, J., and Stouffer, S., "Analyzing the Relative Impact of Spray and Volatile Fuel Properties on Gas Turbine Combustor Ignition in Multiple Rig Geometries," *Aerospace Research Central* (2019), https://doi.org/10.2514/6.2019-1434.
- Soloiu, V., Carapia, C., Smith, R., and Mothershed, D., "RCCI with High Reactivity S8-ULSD Blend and Low Reactivity n-Butanol," in *ICEF Fall Conference*, 2020, https://doi.org/10.1115/1.0003701v.
- 41. Bissada, K., Tan, J., Szymezyk, E., Darnell, M. et al., "Group-Type Characterization of Crude Oil and Bitumen. Part II: Efficient Separation and Quantification of Normal-Paraffins Iso-Paraffins and Naphthenes (PIN)," *Fuel* 173 (2016), https://doi.org/10.1016/j.fuel.2016.01.056.
- 42. Alhikami, A.F., Yao, C.E., and Wang, W.C., "A Study of the Spray Ignition Characteristcis of Hydro-Processed Renewable Diesel, Petroleum Diesel, and Biodiesel Using a Constant Volume Combustion Chamber," *Combustion and Flame* 223 (2021): 55-64, https://doi.org/10.1016/j.combustflame.2020.09.033.
- 43. Shi, H., Uddeen, K., and An, Y., "Statistical Study on Engine Knock Oscillation and Heat Release Using Multiple Spark Plugs and Pressure Sensors," *Fuel* (2021), https://doi.org/10.1016/j.fuel.2021.120746.
- Ryan, T.W., "Correlation of Physical and Chemical Ignition Delay to Cetane Number," SAE Technical Paper 852103 (1985), https://doi.org/10.4271/852103.
- 45. Cheng, C., Cordtz, R., Pedersen, T., and Winther, K., "Investigation of Combustion Characteristics, Physical and Chemical Ignition Delay of Methanol Fuel in a Heavy-Duty Turbo-Charged Compression Ignition Engine," *Fuel* 348 (2023), https://doi.org/10.1016/j.fuel.2023.128536.
- 46. Johnson, C. and Mashuga, C., "Characterizing the Autoignition Behavior of Simple Paraffins and Alcohols; Comparisons and Implications," *Loss Prevention in the Process Industries* (2022), https://doi.org/10.1016/j.jlp.2022.104773.
- 47. Soloiu, V., Weaver, A., and Parker, L., "Constant Volume Combustion Chamber (CVCC) Investigations of Aerospace F-24 and Jet-A in Low-Temperature Heat Release and Negative Temperature Coefficient Regions," *Energy Conversion and Management* (2022), https://doi.org/10.1016/j.enconman.2022.115687.
- 48. Boot, M., Tian, M., Hensen, E., and Sarathy, S., "Impact of Fuel Molecular Structure on Auto-Ignition Behavior Design Rules for Future High Performance Gasolines," *Progress in Energy and Combustion Science* 60 (2017), https://doi.org/10.1016/j.pecs.2016.12.001.
- Curran, H., Gaffuri, P., Pitz, W., and Westbrook, C., "A Comprehensive Modeling Study of n-Heptane Oxidation," Combustion and Flame 114, no. 1-2 (1998), https://doi.org/10.1016/S0010-2180(97)00282-4.
- 50. Curran, H., Gaffuri, P., Pitz, W., and Westbrook, C., "A Comprehensive Modeling Study of Iso-Octane Oxidation," *Combustion and Flame* 129, no. 3 (2002): 253-280, https://doi.org/10.1016/S0010-2180(01)00373-X.

- 51. Farouk, T., Dietrich, D., and Dryer, F., "Three Stage Cool Flame Droplet Burning Behavior on n-Alkane Droplets at Elevated Pressure Conditions: Hot, Warm, and Cool Flame," *Combustion Institute* (2018), https://doi.org/10.1016/j.proci.2018.09.015.
- 52. Kang, S., Dong, W., and Liang, W., "An Experimental Investigation on Two-Stage Low-Temperature Heat Release in Iso-Octane Auto-Ignition," *Combustion and Flame*, https://doi.org/10.1016/j.combustflame.2021.111636.
- 53. Hernandez, J., Bonillo, A., and Ramos, A., "Autoignition of Sustainable Fuels Under Dual Operation with H2-Carriers in a Constant Volume Combustion Chamber," *Fuel*, https://doi.org/10.1016/j.fuel.2023.127487.
- 54. Ju, Y., Reuter, C., Yehia, O., Farouk, T. et al., "Dynamics of Cool Flames," *Progress in Energy and Combustion Science* 75 (2019), https://doi.org/10.1016/j.pecs.2019.100787.
- 55. Waqas, M., Hoth, A., Kolodziej, C., Rockstroh, T. et al., "Detection of Low Temperature Heat Release (LTHR) in the Standard Cooperative Fuel Research (CFR) Engine in Both SI and HCCI Combustion Modes," Fuel 256 (2019).
- 56. Sjoberg, M. and Dec, J., "EGR and Intake Boost for Managing HCCI Low-Temperature Heat Release Over Wide Ranges of Engine Speed," SAE Technical Paper 2007-01-0051 (2007), https://doi.org/10.4271/2007-01-0051.
- 57. Heywood, J.B., Internal Combustion Engine Fundamentals (New York: McGraw Hill, 2018)
- Jurgens, S., Oswald, P., and Selinsek, M., "Assessment of Combustion Properties of Non-Hydroprocessed Fischer-Tropsch Fuels for Aviation," *Fuel Processing Technology* (2019), https://doi.org/10.1016/j.fuproc.2019.05.015.
- Burden, S., Tekawade, A., and Oehlschlaeger, M., "Ignition Delay Times for Jet and Diesel Fuels: Constant Volume Spray and Gas-Phase Shock Tube Measurements," *Fuel* (2018), https://doi.org/10.1016/j.fuel.2018.01.113.
- 60. Eng, J., "Characterization of Pressure Waves in HCCI Combustion," SAE Technical Paper 2002-01-2859 (2002), https://doi.org/10.4271/2002-01-2859.
- 61. Geng, L., Li, S., and Xiao, Y., "Effects of Injection Timing and Rail Pressure on Combustion Characteristics and Cyclic Variations of a Common Rail DI Engine Fueled with F-T Diesel Synthesized from Coal," *Journal of the Energy Institute* 93, no. 6 (2020), https://doi.org/10.1016/j.joei.2020.05.009.
- Zheng, Z., Badawy, T., and Henein, N., "Effect of Cetane Improver on Autoignition Characteristics of Low Cetane Sasol IPK Using Ignition Quality Tester (IQT)," Engineering for Gas Turbines and Power (2013), http://doi.org/10.1115/ ICEF2013-19061.
- 63. Kim, D., Martz, J., and Violi, A., "The Relative Importance of Fuel Oxidation Chemistry and Physical Properties to Spray Ignition," *SAE Int. J. Fuels Lubr.* 10, no. 1 (2017): 10-21, http://doi.org/10.4271/2017-01-0269.
- 64. Palash, S.M., Kalam, M.A., Masjuki, H., Masum, B.M. et al., "Impacts of Biodiesel Combustion on NOx Emissions and Their Reduction Approaches," *Renewable and Sustainable Energy Reviews* 23 (2013): 473-490, https://doi.org/10.1016/j.rser.2013.03.003.
- 65. Heywood, J.B., "Internal Combustion Engine Fundamentals," 1988, 491-567.

- 66. Payri, R., Gimeno, J., Bracho, G., and Vaquerizo, D., "Study of Liquid and Vapor Phase Behavior on Diesel Sprays for Heavy Duty Engine Nozzles," *Applied Thermal Engineering* 107 (2016): 365-378, https://doi.org/10.1016/j.applthermaleng.2016.06.159.
- 67. Westbrook, C.K., "Chemical Kinetics of Hydrocarbon Ignition in Practical Combustion Systems," *Combustion Institute* 28 (2000): 1563-1577, https://doi.org/10.1016/S0082-0784(00)80554-8.

Contact Information

Dr. Valentin Soloiu, Professor,
Director of the Engine Combustion Laboratory
Georgia Southern University
vsoloiu@georgiasouthern.edu

Acknowledgments

The authors would thank to the following for supporting this paper: Air Force Laboratory for providing the fuels, Christopher Mileski, Charles McGuffy from PAC, Michael Rankin, Jacques Lapeyre from PACLP, Joseph von Wolfgang from Malvern Lasers, Coty Harrison from Yokogawa, Sam Olesky from Kistler, Jon Palek from EMS, Whison Chad, Bret MacGregor from MKS Instruments, Arley Bedillion from Mastry engines Center LLC, Stratka Weston and Mealer Christopher from Shimadzu Instruments. Jeffrey Lewis, Enger Paul, David White, Christopher Williams, Tim Domin, Apple Donald, Steven Rougeoau from AVL-NA, Jens Engelhardt and Nelson Zaragoza from MTU-RR,

Study supported by National Science Foundation Grant No. 1950207.

Definitions/Abbreviations

AHRR - Apparent Heat Release

BTDC - Before Top Dead Center

CAD - Crank Angle Degree

CA50 - Crank Angle Degree @ 50% mass burned

CRDI - Common Rail Direct Injection

CD - Combustion Delay

CDC - Conventional Diesel Combustion

CI - Compression Ignition

CO - Carbon Monoxide

CTL - Coal-to-Liquid

CVCC - Constant Volume Combustion Chamber

DCN - Derived Cetane Number

DI - Direct Injection

Dv10 - Largest Droplet Size of 10% of Fuel Spray

Dv50 - Largest Droplet Size of 50% of Fuel Spray

Dv90 - Largest Droplet Size of 90% of Fuel Spray

DTA - Differential Thermal Analysis

EOI - End of Injection

INVESTIGATION OF PERFORMANCE OF FISCHER-TROPSCH COAL-TO-LIQUID FUEL, IPK, IN A COMMON RAIL

FT - Fischer-Tropsch

FTIR - Fourier Transform Spectroscopy

HC - Hydrocarbons

HTHR - High Temperature Heat Release

ID - Ignition Delay

IMEP - Indicated Mean Effective Pressure

IPK - Iso-Paraffinic Kerosene

LHV - Lower Heating Value

LTHR - Low Temperature Heat Release

MC - Main Chamber

N - Engine Speed

NTCR - Negative Temperature Coefficient Region

NOx - Nitrogen oxides

POI - Point of Inflection

PRR - Pressure Rise Rate

Re - Reynolds Number

RPM - Revolutions Per Minute

RI - Ringing Intensity

SOI - Start of Injection

SMD - Sauter Mean Diameter

TA10 - Temperature @ 10% mass vaporized

TA50 - Temperature @ 50% mass vaporized

TA90 - Temperature @ 90% mass vaporized

TGA - Thermogravimetric Analysis

UHC - Unburnt Hydrocarbons

ULSD - Ultra-Low Sulfur Diesel

^{© 2023} SAE International. All rights reserved. No part of this publication may be reproduced, stored in a retrieval system, or transmitted, in any form or by any means, electronic, mechanical, photocopying, recording, or otherwise, without the prior written permission of SAE International.